Desalination and Water Treatment
www.deswater.com
doi: 10.1080/19443994.2015.1038110

57 (2016) 10077–10085
May

Taylor & Francis
Taylor & Francis Group

Application of tubular membranes for surface water treatment: effect of membrane properties and operation modes

Hyeongrak Cho[a], Yong Sun Jang[a], Yunju Jo[a], Yong-Jun Choi[a], Sangho Lee[a,*], Youngkwon Choi[b]

[a]*Department of Civil and Environment Engineering, Kookmin University, Jeongneung-gil 77, Seongbuk-gu, Seoul 136-702, Republic of Korea, Tel. +82 2 910 4529; Fax: +82 2 910 4939; email: sanghlee@kookmin.ac.kr (S. Lee)*
[b]*School of Civil and Environmental Engineering, University of Technology, Sydney, 15 Broadway, Ultimo, New South Wales 2007, Australia*

Received 15 January 2015; Accepted 29 March 2015

ABSTRACT

Filtration characteristics in surface water treatment using tubular microfiltration and ultrafiltration membranes made of polypropylene or ceramic were investigated. A series of filtration experiments were performed to examine the flux behaviors and fouling propensity. When the initial flux was set to be same, the fouling rates were similar regardless of the membrane materials and pore size, suggesting that the hydrodynamic effect was dominant compared with physicochemical interactions between foulants and membranes. Based on theoretical analysis of critical flux, the major foulants were identified to be colloidal particles which size ranges from 0.01 to 0.1 μm. To control the membrane fouling, three methods were compared including (1) periodic backwashing; (2) intermittent operation (periodic pump stop); and (3) the mixed operation of dead end and cross-flow modes. Considering the anti-fouling effect and energy consumption, the mixed operation of dead end and cross-flow modes was better than other operation methods.

Keywords: Ceramic membrane; Tubular membrane; Fouling; Surface water treatment; Critical flux

1. Introduction

The stringent regulation of drinking water quality and a decrease in the clean water sources have led to increased interests in applying microfiltration (MF) and ultrafiltration (UF) for drinking water production [1]. MF membranes completely reject suspended matters including pathogenic microorganisms and turbidity [2,3]. UF membranes can even reject high molecular weight solutes as well as suspended solids, colloids, virus, and macromolecules [4,5]. There are many advantages using MF/UF for drinking water treatment, including increased quality of product water, reduced system footprint, flexibility in operation, and reduced amount of chemicals required for water treatment [6–8].

Currently, hollow fiber MF/UF membranes modules are widely used for drinking water treatment [9,10]. Depending on the application, hollow fiber membranes can be highly practical and cost-effective

*Corresponding author.

Presented at GMVP Desalination Academic Workshop, Seoul, Korea, December 9, 2014

alternatives to conventional chemical and physical separation processes. They offer a compact, cost-effective solution for filtering large volumes of liquids utilizing minimal space and energy [2,9]. However, hollow fiber membrane modules are sensitive to membrane fouling which leads to a decline in water permeability [9,11]. Accordingly, most hollow fiber membrane systems are operated under moderate flux conditions to mitigate fouling [1].

On the other hand, the use of tubular membranes for drinking water is rather limited due to its higher cost than hollow fiber membrane systems. However, tubular membranes are less sensitive to membrane fouling due to their hydrodynamic conditions [12]. Tubular membranes can be produced from ceramic materials as well as polymeric materials, allowing the flexibility of selection for membrane materials. The footprint of the tubular membranes may be reduced by adopting monolith design of the modules. Accordingly, a few membrane plants using tubular ceramic membranes have been constructed and operated.

Although there have been many studies on the use of hollow fiber MF/UF membranes for drinking water treatment [13–17], relatively few works have been done to apply tubular membranes [12,18]. The flux behaviors and fouling propensity may be quite different between hollow fiber and tubular membranes. As shown in Fig. 1, hollow fiber membranes are operated below critical flux condition but tubular membranes are operated near limiting flux conditions. Therefore, a smaller membrane area is required for tubular membranes than hollow fiber membranes. Due to the differences in the hydrodynamic conditions, the operation strategy for tubular membranes should be different from that for hollow fiber membranes [12].

The purpose of this study was to evaluate flux behaviors using tubular MF/UF membranes in surface water treatment under various conditions. A theoretical interpretation of fouling propensity was attempted based on hydrodynamic particle transport model. Three operation strategies to retard membrane fouling, including periodic backwashing, intermittent operation, the mixed operation of dead end, and cross-flow modes, also were compared in terms of fouling rate.

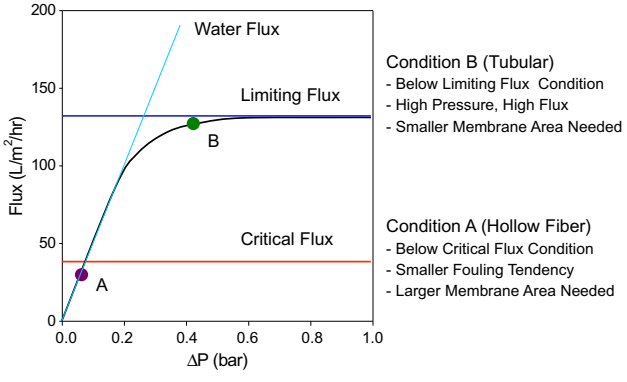

Fig. 1. Comparison of general operation conditions for hollow fiber and tubular membrane modules.

2. Theory

2.1. Mechanisms of particle transport in cross-flow membrane system

In a cross-flow membrane, particle transport depends on two major actions: one action of which is moving the particles toward the membrane surface (negative direction) and the other involves shifting them away from the membrane surface (positive direction). The negative direction forces include van der Waals attraction (F_A), and permeation drag (F_d), while the positive direction actions include electrical double layer repulsion (F_R), Brownian diffusion (F_B), shear-induced diffusion (F_s), and lateral inertial lift (F_l). The gravity and buoyancy forces are equal to zero assuming that the density of particle is same as that of the flowing liquid. The rate of momentum of a particle equals the sum of all the forces imposed on the particles in a fluid stream along a membrane channel. Thus, the net force exerted on a particle along the membrane channel, F, is the sum of all forces noted above [19,20].

$$F = \frac{\pi}{6} d_p^3 \rho_p \frac{dv_p}{dt} = (F_R - F_A) + (F_B + F_s + F_l) - F_d \quad (1)$$

where d_p is the particle diameter; ρ_p is the density of particle; and v_p is the particle transport velocity.

Dividing Eq. (3) by $3\pi\eta d_p$, the particle transport equation can be transformed into the form composed of corresponding velocities.

$$\frac{1}{18} \frac{d_p^3 \rho_p}{\eta} \frac{dv_p}{dt} = (v_R - v_A) + (v_B + v_s + v_l) - J \quad (2)$$

where η is the dynamic viscosity of the feed; v_A is the velocity induced by van der Waals attraction; v_A is the velocity induced by electrical double layer repulsion; v_A is the Brownian diffusion velocity (F_B); v_s is the shear-induced diffusion velocity; v_s is the lateral inertial lift velocity; J is the permeate flux. At a steady state ($dv_p/dt = 0$), the above equation can be simplified to:

$$J_{ss} = v_i + (v_B + v_s + v_l) \quad (3)$$

where v_i is the interaction-induced migration velocity and can be expressed as a difference between repulsive and attractive interaction ($v_R - v_A$). J_{ss} is the steady state flux, which is governed by surface interaction migrations (a) and hydrodynamic back-transport (b). Each of the back-transport velocities may be calculated as the following equations:

$$v_i = \frac{D_B}{\delta} \ln\left(\frac{V_B}{\delta}\right) \quad (4)$$

$$v_B = \frac{0.807 D_B^{2/3} \tau_w^{1/3}}{L^{1/3}} \ln\left(\frac{C_w}{C_b}\right) \quad (5)$$

$$v_s = \frac{0.807 D_s^{2/3} \tau_w^{1/3}}{L^{1/3}} \ln\left(\frac{C_w}{C_b}\right) \quad (6)$$

$$v_l = 0.577 \frac{r_p^3}{l^2} \frac{U_m^2}{v} \quad (7)$$

where D_B represents the Brownian diffusion coefficient ($=k_B T/6\pi\mu r_p^2$); D_s the shear-induced diffusion coefficient ($=0.03\ r_p^2 \tau_w$); δ the boundary layer thickness; V_B the potential barrier between particle and membrane; C_w the particle concentration at membrane surface; C_b the particle concentration at bulk solution; L the membrane length; l the channel height; v the kinematic viscosity of the dispersing medium; U_m the maximum flow velocity at channel entrance; r_p the radius of particle. Thus, the steady state flux can be estimated from Eq. (3) since the steady state flux corresponds to the critical flux at which no additional particle deposition takes place with time.

3. Materials and methods

3.1. Feed water

Raw water samples used in this study were collected from Han River, Pungnap intake (the water supply source for Seoul, Korea). Samples were stored in a refrigerator without any chemical pretreatment before being used in the test system. The pH, DOC, and turbidity of the samples did not change significantly during storage. Some key water quality characteristics are presented in Table 1.

3.2. Membranes

A few MF and UF membranes were tested for surface water treatment. Both polymeric and ceramic membranes were used. Details on these pretreatment processes are given in Table 2.

3.3. System operation

The configuration of the experimental apparatus with a cross-flow filtration is shown in Fig. 2. The system consists of a feed tank with a total working volume of 10 L, a vane pump for the recirculation of retentate, and a tubular membrane module. The transmembrane pressure inside the module was regulated to a desired value using the back pressure valve. The fluid velocity through the membrane channel was adjusted by controlling the speed of the pump motor with an electrical inverter (Goldstar Starverter-G, Korea). The retentate and permeate from the MF/UF loop were returned to the feed tank to maintain a constant working. The permeate was collected in a reservoir on the electronic balance, and the data were collected on a personal computer. The feed water was maintained at a temperature of 25℃ by a water jacket in order to minimize the effect of temperature on the filtration results.

3.4. Analytical methods

TOC, ion concentration, and suspended solid contents for raw water and membrane permeate were analyzed using the procedures described in the Standard method [21]. Particle size and the distribution of solids present in the feed water and retentate were measured using a light scattering instrument (Malvern MasterSizer/E, UK). The zeta potential of solids in the feed water was analyzed with a zeta potential analyzer (Coulter Delsa 440SX, USA).

4. Results and discussion

4.1. Effect of membrane materials on flux decline

Fig. 3 shows flux vs. time behaviors during the cross-flow filtration of untreated raw water. Four different membranes with a similar pore size were compared, including Zr–C ceramic membrane (0.14 μm), polypropylene membrane (0.2 μm), Zr–Al ceramic membrane (0.1 μm), and Al ceramic membrane (0.1 μm). The cross-flow velocity was set to be 1.2 m/s. The initial flux was adjusted to be similar (ranging from 225 to 275 L/m^2 h) by applying different transmembrane pressures. Since the Zr–C membrane has lower water permeability, a higher pressure (1.0 bar) was applied. For the other membranes, the transmembrane pressure of 0.2 bar was applied. Although different

Table 1
Water quality parameters for raw water samples

	Minimum	Maximum	Average
SS (mg/L)	3.5	7.5	5.5
Turbidity (NTU)	2.0	9.0	5.0
TOC (mg/L)	1.5	3.1	2.3
UV_{254} (cm^{-1})	0.023	0.053	0.043
SUVA ($m^{-1}L/mg$)	1.5	1.8	1.7
THMFP (μg/L)	66	72	70
HPC (CFU/100 mL)	4.0×10^4	6.0×10^4	5.0×10^4
Ca (mg/L)	10	20	10.5
Mg (mg/L)	3	4	3.3
Fe (mg/L)	0.0	0.06	0.05
Mn (mg/L)	0.0	0.02	0.01
Average zeta potential (mV)	−9.5	−11.3	−10

Table 2
Summary of the tubular MF and UF membranes

Type	Maker	Trade name	Pore size	Material	Permeability ($L/m^2/h/bar$)
Microfilter	Microdyne	MD020TP2N	0.2 μm	Polypropylene	1,500
	SCT	Membralox A200	0.2 μm	Alumina	1,500
	SCT	Membralox Z100	0.1 μm	Zirconia skin Alumina support	1,500
	Techsep	Carbosep M14	0.14 μm	Zirconia skin Carbon support	400
Ultrafilter	Techsep	Carbosep M3	MWCO 150,000	Zirconia skin Carbon support	200
	Techsep	Carbosep M8	MWCO 50,000	Zirconia skin Carbon support	190

membranes were used, the flux behaviors seem to be similar. The initial flux was over 200 L/m^2 h but the final flux after 800 min was approximately 75 L/m^2 h, indicating that the hydraulic resistance increases by 2.7 times.

It is interesting to note that the difference in membrane materials does not affect the flux behaviors. The polypropylene membrane was more hydrophobic than ceramic membranes. The zirconia and aluminum also have different surfaces properties. However, the fouling rates were almost identical if the initial flux and cross-flow velocity were maintained constant. This suggests that membrane fouling due to physicochemical interactions between foulants and membrane materials was less important than that due to hydrodynamic effects such as particle deposition and cake formation.

4.2. Effect of pore size and molecular weight cutoff on flux behavior

In Fig. 4, the Zr–C membranes with different pore size or molecular weight cutoff were compared. The cross-flow velocity was set to be 1.2 m/s and the initial flux was adjusted to be same. The results were similar to the previous experiments. The flux decreases from 230 to 75 L/m^2 h after 800 min. Again, the pore size and molecular weight cutoff did not affect the flux behavior. If the fouling occurs by pore blocking, the fouling propensity between MF and UF should be different. Accordingly, it seems that the pore blocking is not a dominant mechanisms for membrane fouling. Instead, the formation of cake layer by particle deposition is likely to be more important.

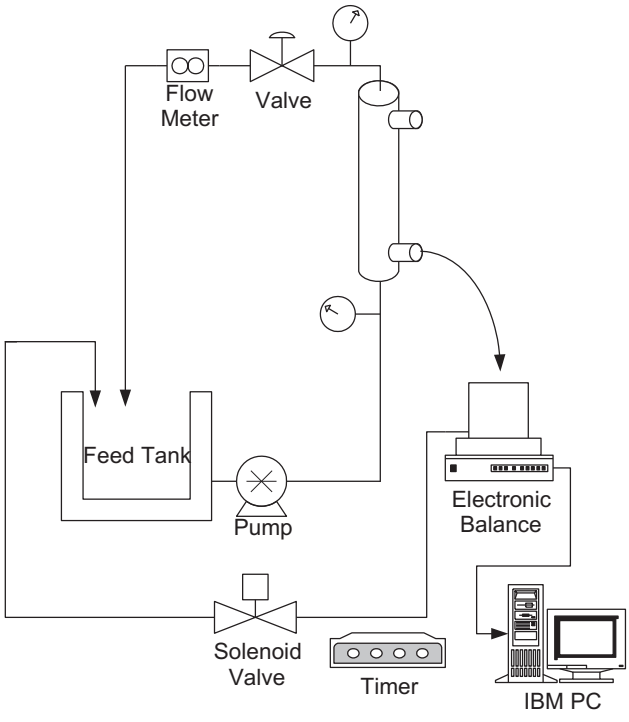

Fig. 2. Schematic diagram for tubular membrane system.

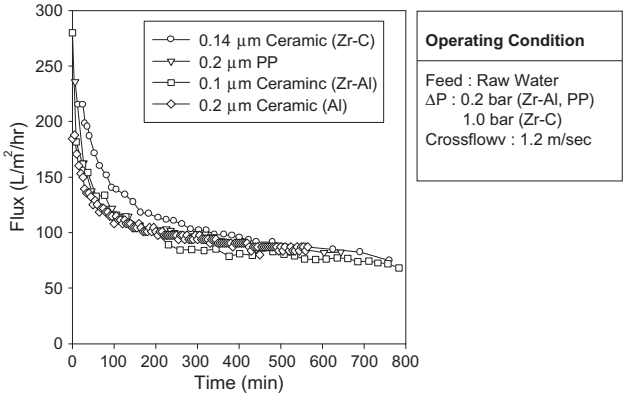

Fig. 3. Effect of membrane materials on flux behaviors in tubular MF membranes.

4.3. Estimation of critical flux

Although tubular membranes are operated above the critical flux, it is important to measure critical flux to estimate fouling potential of the feed water. Accordingly, two approaches were applied to measure the critical flux including flux step method and calculation of back-transport velocity. Fig. 5 shows the results of the flux step method for experimental determination of the critical flux. The transmembrane pressure was

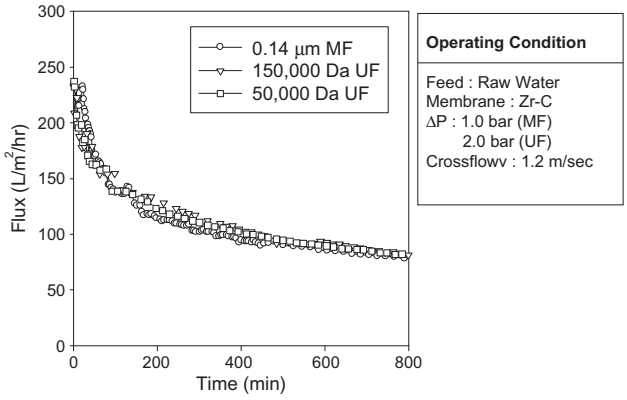

Fig. 4. Effect of pore size on flux behaviors in tubular MF and UF membranes.

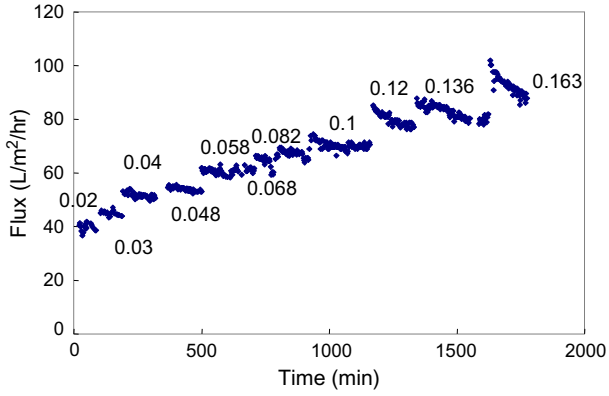

Fig. 5. Experimental determination of critical flux (membrane: PP; cross-flow velocity: 1.2 m/s).

increased stepwise and the changes in flux with time were measured. Although the starting flux was relatively low (40 L/m^2 h), the flux decline occurred from the beginning. These results suggest that the critical flux was lower than 40 L/m^2 h.

The theoretical calculation of the critical flux based on particle back-transport velocity was also attempted. In Eqs. (4)–(7), particle transport is expressed as a function of hydrodynamic back-transport and permeation drag (flux) because the diffusion coefficients (D_B and D_S) and potential barrier (V_B) are dependent on the particle radius, r_P. As described above, the net back-transport velocity of a particle is the sum of various velocity components, including Brownian diffusion, shear-induced diffusion, and lateral migration. Fig. 6 shows the profiles of the back-transport velocities with different particle sizes and fluid velocities, indicating the particle transport and deposition is greatly dependent on its size. The net particle

back-transport velocity exhibited a minimum at a particle diameter of approximately 0.2 μm, although it is somewhat changeable with the variations in fluid velocity. Based on this calculation, the theoretical critical flux was 35 L/m^2 h.

4.4. Effect of cross-flow velocity on flux behavior

Since the hydrodynamic effect is important in the tubular MF/UF membranes, the cross-flow velocity significantly affects the fouling propensity. Fig. 7 shows the results of MF experiments using polypropylene membranes under various cross-flow conditions. The applied pressure was set to 0.2 bar. It is evident from the graph that the final flux increases with an increase in cross-flow velocity. At low cross-flow velocities, the flux decrease to 50 L/m^2 h after 500 min. At higher cross-flow velocities, the final flux was higher than 100 L/m^2 h even after 600 min. These results confirm the importance of cross-flow velocity in the tubular membrane systems.

The different fouling behaviors can be explained by comparing the critical flux values at different cross-flow velocities. As illustrated in Fig. 8, the minimum value for the back-transport velocity increases with increasing the cross-flow velocity. In other words, the critical flux increases with cross-flow velocity. However, it should be also noted that the critical flux cannot be sufficiently high even above the cross-flow velocity of 2.1 m/s. Considering the energy consumption to create high cross-flow velocity, it is not likely to completely control fouling by increasing the cross-flow velocity. Therefore, different approaches to reduce fouling and reduce energy consumption are required.

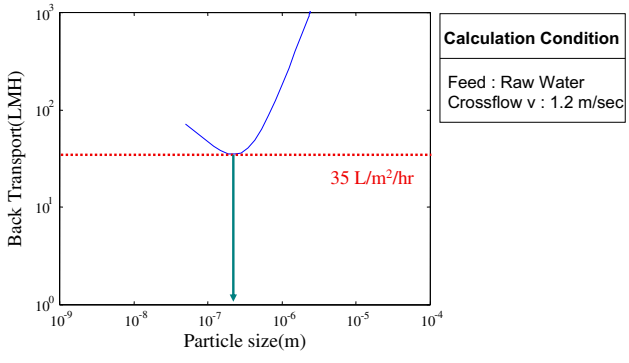

Fig. 6. Theoretical calculation of critical flux (membrane: PP; cross-flow velocity: 1.2 m/s).

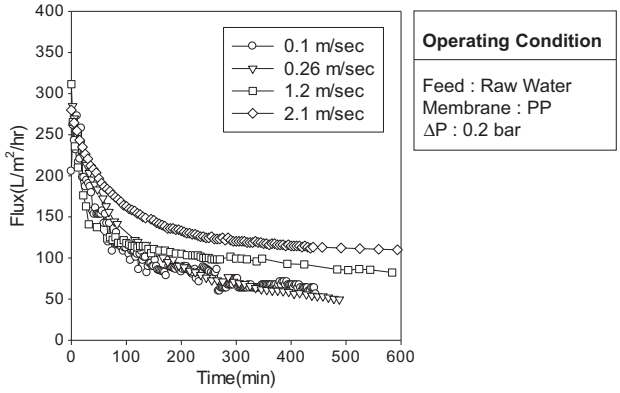

Fig. 7. Effect of cross-flow velocity on flux behaviors in tubular MF membranes.

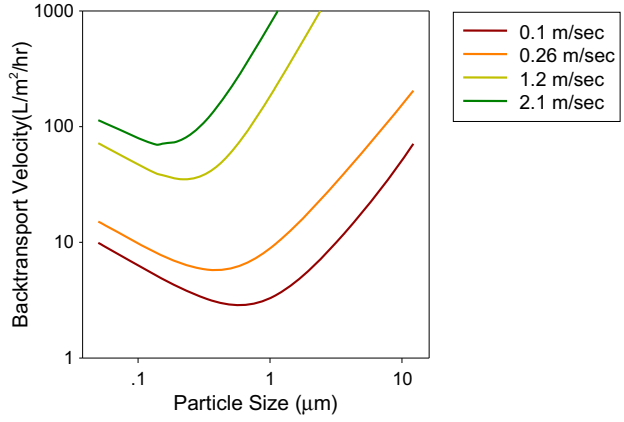

Fig. 8. Calculation of critical flux at various cross-flow velocity.

4.5. Comparison of means to reduce membrane fouling

Three types of the strategies to control membrane fouling were compared: periodic backwashing, intermittent operation; the mixed operation of dead end; and cross-flow modes. Fig. 9 illustrates the concept of backwashing, intermittent operation, and the mixed operation. In backwashing, the deposited foulants are removed by reversing the permeate flow. In the intermittent operation, the foulant layers are depressurized when the pump stops. In the mixed operation, the cake layers formed in the dead end mode are washed out in the cross-flow filtration mode.

Fig. 10 shows the results of filtration with periodic backwashing. Without backwashing, the fouling rate was relatively high. As the backwash interval decreases, the fouling rate was reduced. The average flux increased by 20–40% with periodic backwashing at 1 bar. However, it should be also noted that

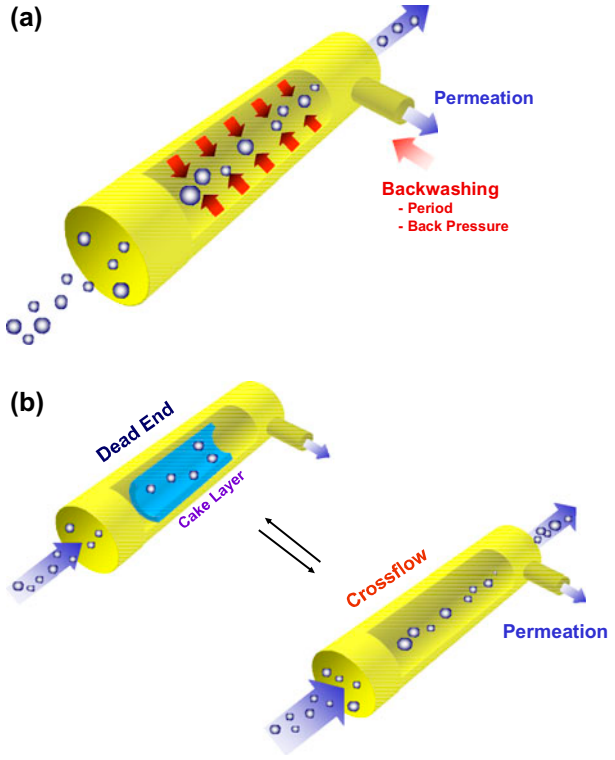

Fig. 9. Two operation modes (a) cross-flow filtration with periodic backwashing and (b) mixed operation of dead end and cross-flow modes.

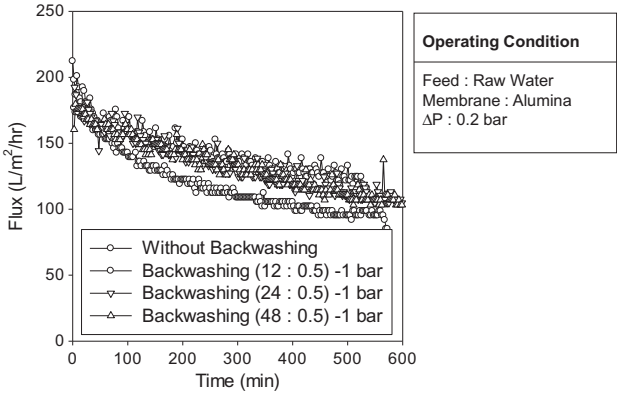

Fig. 10. Effect of backwash frequency on flux behavior in tubular MF membrane.

frequent backwashing leads to lower recovery of permeate as well as higher energy consumption. For instance, the backwashing for 0.5 min at 1 bar in every 12 min results in a reduction in permeate recovery by 20%. Accordingly, the increase in net flux by applying backwashing in this case was not significant.

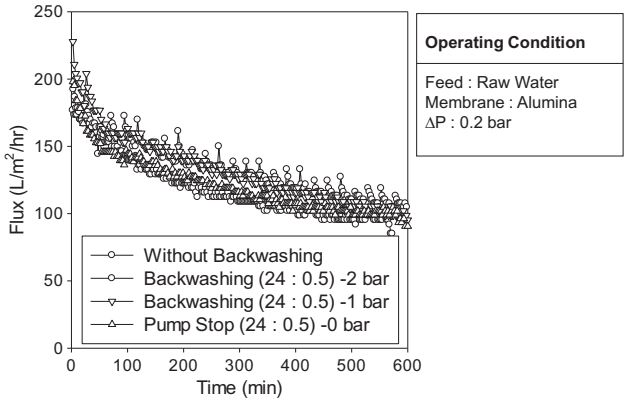

Fig. 11. Comparison of two operation modes: periodic backwashing and pump stop.

Fig. 11 shows the effect of backwashing pressure on the flux. The period of backwashing was set constant at 24 min (filtration) and 0.5 min (backwashing). When the pressure was set at 0 bar, the pump stopped and no additional pressure was applied for backwashing. It is evident from the figure that the flux increases with an increase in backwashing pressure. The pump stop (backwashing at 0 bar) did not show any effect. This suggests that the intermittent operation by pump stop is not effective to increase flux in this case.

In Fig. 12, the results of the mixed operation of dead end and cross-flow filtration modes were shown. The flux increases significantly with the application of the mixed operation method. The fouling rate was even lower than that of cross-flow filtration, implying that the foulant layers are continuously removed by applying two different filtration modes. Since the energy consumption of the dead end filtration mode is

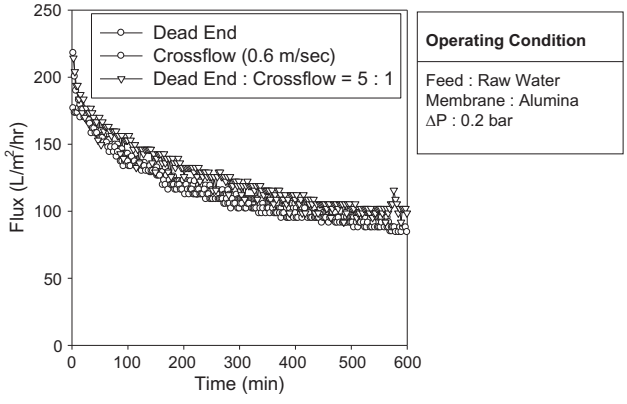

Fig. 12. Effect of mixed operation of dead end and cross-flow modes on flux decline.

lower than cross-flow filtration mode, the mixed operation mode seems to be effective in terms of energy consumption and fouling control.

5. Conclusion

In this work, the flux behaviors of tubular MF/UF membranes were investigated under various conditions. The following conclusions were drawn:

(1) Under similar hydrodynamic conditions including initial flux and cross-flow velocity, the fouling rates were similar regardless of membrane materials. This suggests that the hydrodynamic effect is more important that physicochemical interactions between foulants and membrane surface.
(2) The difference in pore size or molecular weight cutoff did not affect the fouling rate under same initial flux and cross-flow velocity. This suggests that the major fouling mechanism is not pore blocking but cake formation.
(3) The effect of cross-flow velocity on fouling rate could be interpreted by applying the concept of the critical flux. The particles ranging from 0.01 to 0.1 μm seem to be the main reason to cause fouling.
(4) Three types of the strategies to control membrane fouling were compared, including periodic backwashing, intermittent operation; the mixed operation of dead end; and cross-flow modes. Although periodic backwashing was effective, it may lead to increased energy consumption and lower recovery. Although the intermittent operation was relatively ineffective, the mixed operation method was found to be efficient to reduce both fouling and energy consumption.

Acknowledgement

This research was supported by a grant (code 13IFIP-B065893-01) from Industrial Facilities & Infrastructure Research Program funded by Ministry of Land, Infrastructure and Transport of Korean government and also supported by a grant (code 12-TI-C01) from Advanced Water Management Research program by Ministry of Land, Infrastructure.

References

[1] C. Liu, 2.5—Advances in membrane technologies for drinking water purification, in: S. Ahuja (Ed.), Comprehensive Water Quality and Purification, Elsevier, Waltham, MA, 2014, pp. 75–97.
[2] A.G. Fane, C.Y. Tang, R. Wang, 4.11—Membrane technology for water: Microfiltration, ultrafiltration, nanofiltration, and reverse osmosis, in: P. Wilderer (Ed.), Treatise on Water Science, Elsevier, Oxford, 2011, pp. 301–335.
[3] L.J. Zeman, A.L. Zydney, Microfiltration and Ultrafiltration—Principles and Applications, Marcel Dekker, New York, NY, 1996, p. 618.
[4] L. Bai, F. Qu, H. Liang, J. Ma, H. Chang, M. Wang, G. Li, Membrane fouling during ultrafiltration (UF) of surface water: Effects of sludge discharge interval (SDI), Desalination 319 (2013) 18–24.
[5] R.K. Patrick, Weber, ultrafiltration of surface water with ®MOLPURE FW50 hollow fibre module, Desalination 119 (1998) 335–339.
[6] X. Fan, Y. Tao, L. Wang, X. Zhang, Y. Lei, Z. Wang, H. Noguchi, Performance of an integrated process combining ozonation with ceramic membrane ultrafiltration for advanced treatment of drinking water, Desalination 335 (2014) 47–54.
[7] T. Hirata, A. Hashimoto, Experimental assessment of the efficacy of microfiltration and ultrafiltration for Cryptosporidium removal, Water Sci. Technol. 38 (12) (1998) 103–107.
[8] K. Kimura, K. Tanaka, Y. Watanabe, Microfiltration of different surface waters with/without coagulation: Clear correlations between membrane fouling and hydrophilic biopolymers, Water Res. 49 (2014) 434–443.
[9] S. Lee, P.-K. Park, J.-H. Kim, K.-M. Yeon, C.-H. Lee, Analysis of filtration characteristics in submerged microfiltration for drinking water treatment, Water Res. 42(12) (2008) 3109–3121.
[10] A. Yuasa, Drinking water production by coagulation–microfiltration and adsorption–ultrafiltration, Water Sci. Technol. 37(10) (1998) 135–146.
[11] J.-Y. Tian, Y.-P. Xu, Z.-L. Chen, J. Nan, G.-B. Li, Air bubbling for alleviating membrane fouling of immersed hollow-fiber membrane for ultrafiltration of river water, Desalination 260 (2010) 225–230.
[12] M. Bodzek, K. Konieczny, Comparison of ceramic and capillary membranes in the treatment of natural water by means of ultrafiltration and microfiltration, Desalination 119 (1998) 191–197.
[13] H.-S. Kim, S. Takizawa, S. Ohgaki, Application of microfiltration systems coupled with powdered activated carbon to river water treatment, Desalination 202 (2007) 271–277.
[14] K. Konieczny, D. Sąkol, J. Płonka, M. Rajca, M. Bodzek, Coagulation–ultrafiltration system for river water treatment, Desalination 240 (2009) 151–159.
[15] M. Li, G. Wu, Y. Guan, X. Zhang, Treatment of river water by a hybrid coagulation and ceramic membrane process, Desalination 280 (2011) 114–119.

[16] B. Schlichter, V. Mavrov, H. Chmiel, Study of a hybrid process combining ozonation and microfiltration/ultrafiltration for drinking water production from surface water, Desalination 168 (2004) 307–317.
[17] Y. Song, B. Dong, N. Gao, S. Xia, Huangpu River water treatment by microfiltration with ozone pretreatment, Desalination 250 (2010) 71–75.
[18] P. Belibi Belibi, M.M.G. Nguemtchouin, M. Rivallin, J. Ndi Nsami, J. Sieliechi, S. Cerneaux, M.B. Ngassoum, M. Cretin, Microfiltration ceramic membranes from local Cameroonian clay applicable to water treatment, Ceramics Int., 41(2, Part B) (2015) 2752–2759.
[19] S. Lee, C.-H. Lee, Effect of membrane properties and pretreatment on flux and NOM rejection in surface water nanofiltration, Sep. Purif. Technol. 56(1) (2007) 1–8.
[20] S.-H. Yoon, C.-H. Lee, K.-J. Kim, A.G. Fane, Three-dimensional simulation of the deposition of multi-dispersed charged particles and prediction of resulting flux during cross-flow microfiltration, J. Membr. Sci. 161 (1999) 7–20.
[21] APHA, AWWA, WEF, Standard Methods for the Examination of Water and Wastewater, AWWA, New York, NY, 2012.